applied sciences

MDPI

Article

Seismic Damage Evaluation of Concrete-Encased Steel Frame-Reinforced Concrete Core Tube Buildings Based on Dynamic Characteristics

Lei Zeng *, Yunfeng Xiao, Yiguang Chen, Siqian Jin, Wei Xie and Xianjie Li

School of Urban Construction, Yangtze University, Jingzhou 434023, China; xyf19910909@126.com (Y.X.); cyg19920907@126.com (Y.C.); jinsiqian0220@163.com (S.J.); xiewei0202@126.com (W.X.); lixianjiexy@126.com (X.L.)

* Correspondence: zenglei@yangtzeu.edu.cn; Tel.: +86-138-7235-9779

Academic Editors: Gangbing Song, Dimitrios G. Aggelis and Stefano Invernizzi
Received: 8 December 2016; Accepted: 16 March 2017; Published: 23 March 2017

Abstract: To evaluate damage state and residual resistance of concrete-encased steel frame-reinforced concrete core tube buildings under earthquake actions, a criterion of damage assessment based on dynamic characteristics is proposed in this paper. Dynamic characterization experiments were conducted on a 10-story and 1/5 scaled building model using velocity sensors on each floor, and natural frequencies were obtained based on the measured data. Modal analysis was carried out using a nonlinear finite element program, and the simulation results of the dynamic characteristics agreed well with experimental ones. Then, the damage processes under different seismic wave inputs were revealed based on finite element analysis, and the max story drift angle was chosen to reflect the damage state and to quantify the degree of damage. A criterion of seismic damage assessment is proposed based on the relationship between the quantitative damage value and the dynamic characteristics, in which the higher order modes were considered. Moreover, influencing factors, including earthquake intensity and structural stiffness ratio, were analyzed, and the results indicated that the proposed damage index based on dynamic characteristics can account for the higher-order modes and provides an innovative approach to evaluate the seismic damage.

Keywords: damage evaluation; earthquake; concrete encased structures; dynamic characteristics

1. Introduction

Concrete-encased composite structures are widely used in high-rise buildings owing to their excellent seismic performance, high rigidity and low cost. The hybrid structural systems with concrete-encased composite frames and reinforced concrete core tubes have been adopted in many super high-rise buildings especially in the US [1], China [2] and Japan [3,4].

Many studies have been performed on hybrid structural systems by large-scale pseudo-static tests, pseudo-dynamic tests and shaking table tests to investigate the fundamental mechanisms and seismic behavior. The research objects included hybrid structural systems consisting of steel frames, concrete-encased steel frames, and concrete-filled steel tubes [5–10]. They attempted to understand the seismic response, seismic behavior and failure characteristics of the hybrid structural system. However, such tests are very expensive and even the largest shaking table in the world cannot simulate the damage process of full-scale super high-rise buildings. As an alternative, numerical simulations based on accurate models have been widely accepted as an important technique to study earthquake-induced structural behavior, by which the entire dynamical catastrophe processes from material damage and local failure to integral collapse can be replicated to a certain extent [11–15].

The results of the above mentioned experiments and simulations indicated that a well-designed frame-core tube structural system possesses good seismic performance, but unfavorable failure mode can still occur in some states. As the two parts that resist lateral force, the frame and the core tube, cooperatively operate with different stiffness, an unequal distribution of shear in the two components is caused [16,17]. To effectively prevent earthquake-induced structural collapse, the damage stage and the residual bearing capacity of structures should be properly predicted in this structural system.

A seismic damage model actually reflecting strength and stiffness degradation under cyclic loading is the basis of structural safety margin evaluation and post-earthquake restoration. Based on the initial strength criterion and deformation, seismic damage assessment models based on energy criteria were proposed [18,19]. Afterwards, the losses of motion stability and the loss of vertical bearing capacity were taken as criterions to judge the collapse of structures [20]. A stress wave-based active sensing method was also used to detect damage in concrete structures [21–27]. The piezoelectric smart aggregates were adopted for structural health monitoring [28–30]. However, the existing criterions cannot reflect the influence of loading amplitude and loading path on the cumulative damage of the structures. Since the damage and collapse of a structure is a complex dynamic instability problem, collapse criterion and damage evaluation index on the level of the overall structure should be developed and be applied to concrete-encased steel frame-reinforced concrete core tube structures.

In this paper, a 1/5 scale and 10-storey concrete encased steel frame-reinforced concrete core tube building model was constructed according to the design code of China (GB50023-2009). The prototype structure was designed with 8 degrees of seismic fortification. The specimen was measured for a proposed criterion of seismic damage assessment. Dynamic characterization experiments were conducted using velocity sensors on each floor. The natural frequencies were obtained based on the experimental data. Modal analysis was also carried out using a nonlinear finite element program based on a fiber model in OpenSees. The modal analysis considered geometric nonlinearity and material nonlinearity. Then, the damage process under different seismic wave input was revealed based on finite element analysis, and the max story drift angle was chosen to reflect the damage state and to quantify the damage degree. The structural dynamic characteristics indexes such as vibration modes and frequencies can be well detected according to non-destructive structure. A criterion of seismic damage assessment was proposed based on the relationship between the quantitative damage value and dynamic characteristics. The author hopes to provide references for damage evaluation, structural health monitoring and post-earthquake restoration of concrete-encased steel frame-reinforced concrete core tube buildings.

2. Experimental Program

2.1. Details of Specimen

The experimental specimen was constructed in the Civil Engineering Experimental Center of Yangtze University (Jingzhou, China). The specimen was a model of a concrete encased steel frame-reinforced concrete core tube built in an 8-degree seismic fortification intensity zone. The model was 1/5 reduced-scale of 10 stories with a total height of 8700 mm. To ensure experimental safety, the slab of the top floor was not constructed. The planar of specimen was a square with dimensions of 1800 mm × 1800 mm. The depth of the foundation, the first story and the rest of the stories were 500 mm, 1000 mm and 800 mm respectively. The specimen consisted of a concrete encased steel frame and a reinforced concrete core tube. The steel skeleton was pre-buried inside the foundation, as shown in Figure 1.

The concrete-encased steel frame system consisted of 12 concrete-encased columns with cruciform section and 20 steel beams on each story. As shown in Figure 2, the longitudinal bars in columns were 4 mm in diameter. As shown in Figure 3a, steel beams were rigidly connected with columns and the substantial details of specimen were shown in Figure 3b.

The reinforced concrete core tube was 600 mm × 600 mm in square. The core tube in first two stories was 60 mm in thickness and for the rest it measured 40 mm. Two holes with 500 mm × 300 mm in dimension were set on each story to simulate the elevator doors. Double-layer meshed bars were set in the edge of the holes as shown in Figure 4a. The internal steel mesh reinforcement and the view of reinforced concrete core tube were shown in Figure 4b. Concealed columns were pre-buried in the corners of core tube, which improved the bearing capacity and was beneficial to the connection between beams and columns. The thickness of floor slabs is 30 mm.

Premixed concrete was used. To determine the average concrete compressive strength three cylinders (150 × 300 mm) were tested. The measured concrete compressive strength was 41.5 MPa. The longitudinal bars and hoop reinforcements used were 4 mm in diameter. The results of the characterization tests are shown in Table 1.

Table 1. Materials properties of steel.

Material	Yield Strength f_y (N/mm^2)	Ultimate Strength f_u (N/mm^2)	Elastic Modulus E_s (N/mm^2)
Φ4 bars	305	424	2.1×10^5
Steel plate	327	463	2.0×10^5

According to Architectural Structure Load Standards (GB50009-2001) of China, live and dead load were considered as 2.0 kN/m^2 and 1.6 kN/m^2 respectively, which took the weight of filler wall into account. Appropriate combination of the loads was calculated and achieved by preloading sandbags on each floor. The design of the concrete-encased steel frame-reinforced concrete core tube building was governed by the earthquake actions.

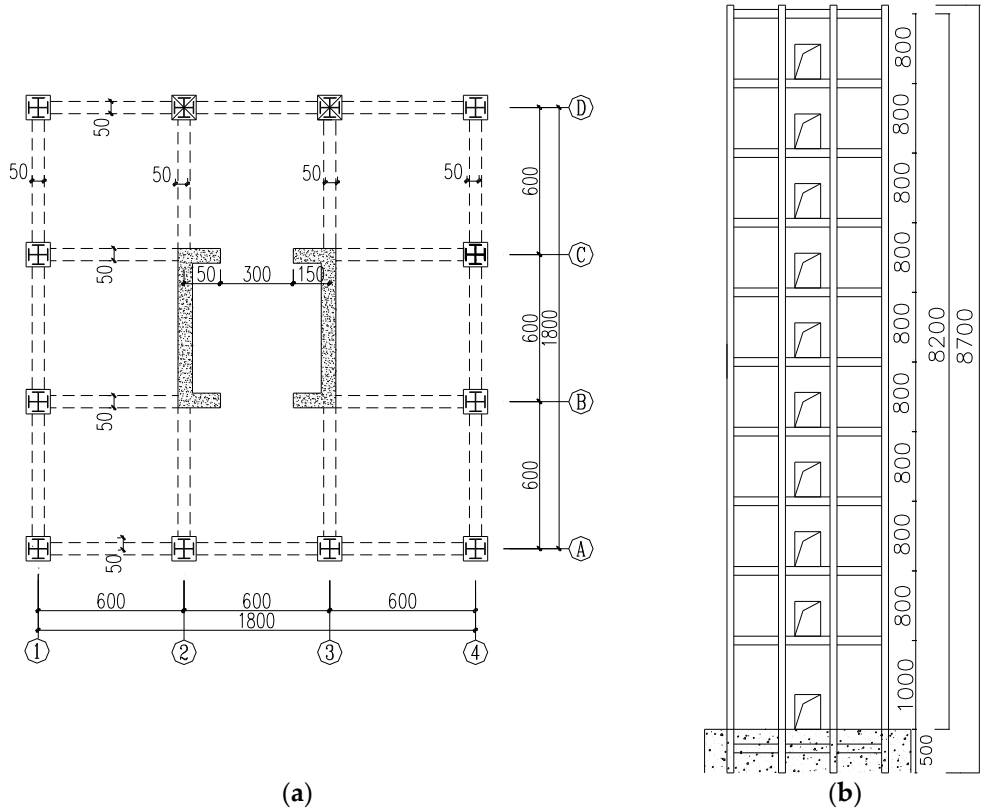

Figure 1. Dimension of specimen: (**a**) cross section; (**b**) elevation (unit: mm).

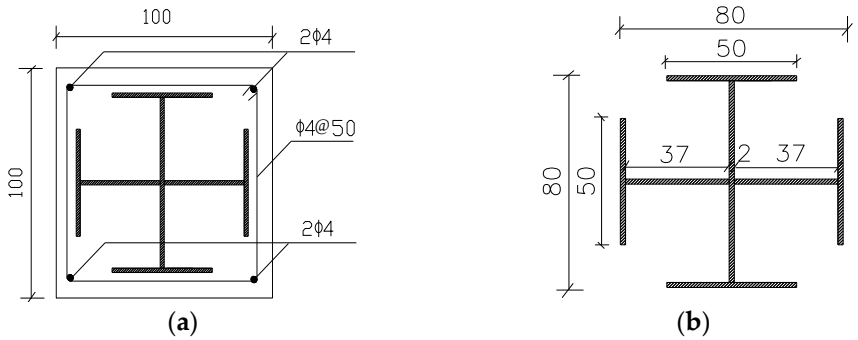

Figure 2. (**a**) Column section and dimension; (**b**) dimension of steel skeleton (unit: mm).

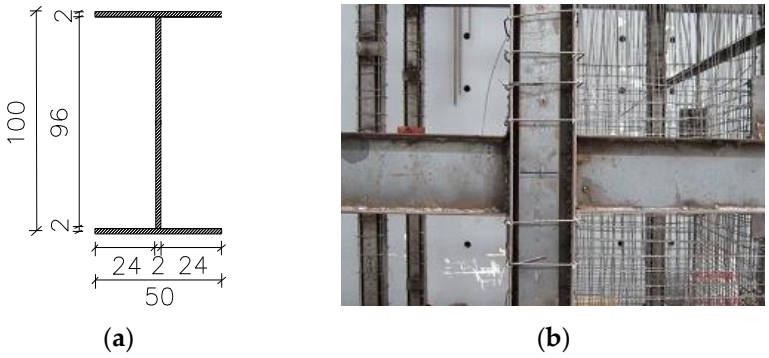

Figure 3. (**a**) Beam cross-section; (**b**) beam-column connection (unit: mm).

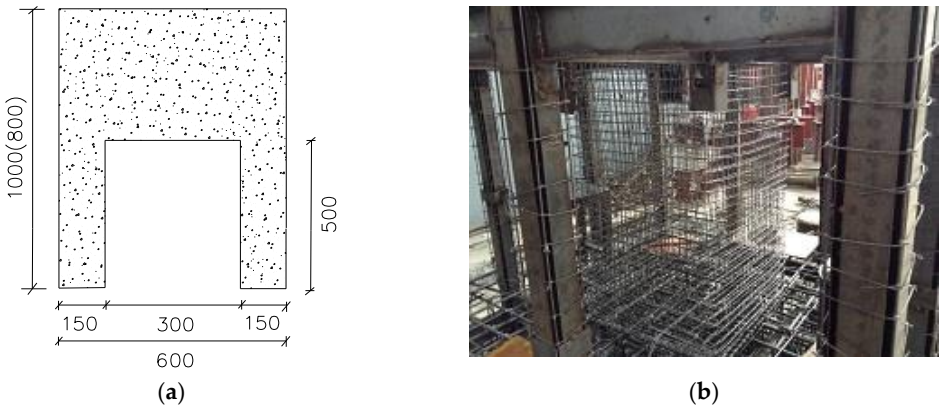

Figure 4. (**a**) Shear wall with an opening; (**b**) details of Shear wall (unit: mm).

2.2. Test Setup and Procedure

The pulsation method was applied to measure the dynamic characteristics of the specimen. Vibration pickup sensors (China Orient Institute of Noise & Vibration, Beijing, China) were installed on the center of each floor, which took the earth pulse as the vibromotive source as shown in Figure 5. The vibration pickup sensors and signal acquisition system were shown in Figure 5d; two measurements were taken for accurate results. The sensors were applicable for structures with low natural frequency at the range of 2 Hz to 100 Hz. Due to the symmetry of the cross section, vibration modes in only one horizontal direction were measured. As shown in Figure 6, data collected from the sensors indicated a resonance phenomenon at f_0 = 5.942 Hz, which showed the primary frequency.

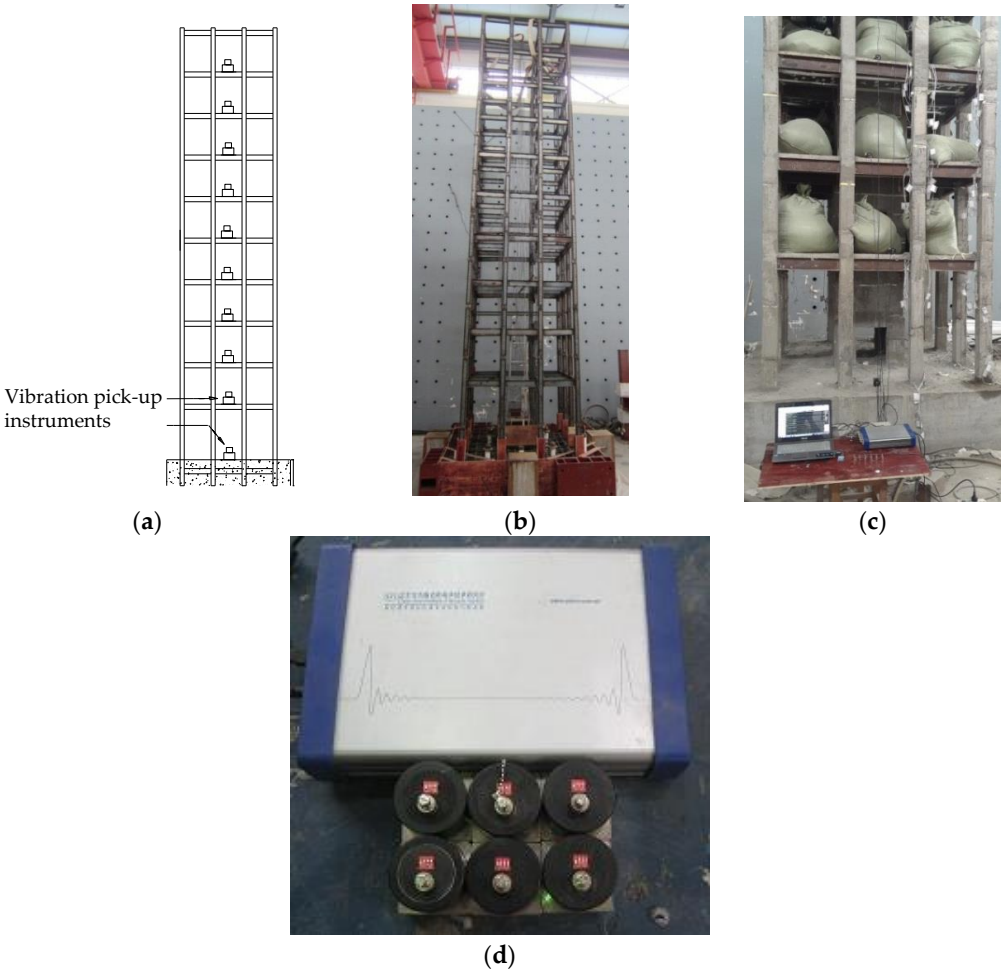

Figure 5. (**a**) Arrangement of vibration pick-up instruments; (**b**) the steel skeleton; (**c**) measurement instrument; (**d**) details of the instrument.

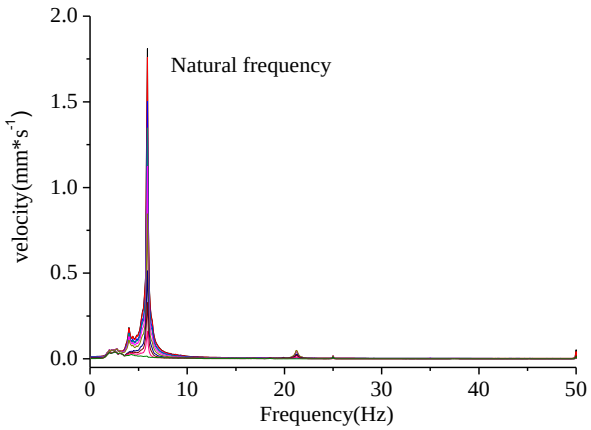

Figure 6. Natural frequency.

Furthermore, modal analyses of higher order frequencies based on the measured datas were conducted by the Data Acquisition and Signal Processing (DASP) program. The principle and procedure are shown as the follows [31,32].

Dynamic characteristics for structure can be expressed by the dynamic equation.

$$\boldsymbol{M}\ddot{x} + \boldsymbol{C}\dot{x} + \boldsymbol{K}x = \boldsymbol{f}(t) \tag{1}$$

where $\boldsymbol{M}$, $\boldsymbol{C}$ and $\boldsymbol{K}$ are matrices of mass, damping and stiffness, respectively; x, $\dot{x}$ and $\ddot{x}$ are the response vectors of displacement, velocity and acceleration, respectively; $\boldsymbol{f}(t)$ is the vector of exciting force.

Laplace transform method is applied on Equation (1).

$$\left[\boldsymbol{M}s^2 + \boldsymbol{C}s + \boldsymbol{K}\right]\boldsymbol{X}(s) = \boldsymbol{F}(s) \tag{2}$$

where s is a complex variable.

The matrix of generalized impedance $\boldsymbol{Z}(s)$ can be expressed as:

$$\boldsymbol{Z}(s) = \left[\boldsymbol{M}s^2 + \boldsymbol{C}s + \boldsymbol{K}\right] \tag{3}$$

The matrix of frequency response $\boldsymbol{H}(s)$ can be expressed as:

$$\boldsymbol{H}(s) = \left[\boldsymbol{M}s^2 + \boldsymbol{C}s + \boldsymbol{K}\right]^{-1} \tag{4}$$

When $s = jf$, jf is column matrix of frequency at j-column. Equation (3) can be expressed as:

$$\boldsymbol{Z}(f) = \left(\boldsymbol{K} - f^2\boldsymbol{M}\right) + jf\boldsymbol{C} \tag{5}$$

Matrix of vibration mode can be expressed as:

$$\Phi = [\phi_1, \phi_2, \cdots, \phi_n] \tag{6}$$

where ϕ_n is the n-order of vibration mode.

A symmetric matrix has weighting orthogonal characteristic, and $\boldsymbol{M}$, $\boldsymbol{C}$ and $\boldsymbol{K}$ are respectively expressed as:

$$\boldsymbol{\Phi}^T\boldsymbol{M}\boldsymbol{\Phi} = \begin{pmatrix} \ddots & & \\ & m_r & \\ & & \ddots \end{pmatrix} \tag{7}$$

$$\boldsymbol{\Phi}^T\boldsymbol{C}\boldsymbol{\Phi} = \begin{pmatrix} \ddots & & \\ & c_r & \\ & & \ddots \end{pmatrix} \tag{8}$$

$$\boldsymbol{\Phi}^T\boldsymbol{K}\boldsymbol{\Phi} = \begin{pmatrix} \ddots & & \\ & k_r & \\ & & \ddots \end{pmatrix} \tag{9}$$

where m_r, c_r and k_r are mass, damping and stiffness at r-order.

According to Equations (7)–(9), Equation (5) can be expressed as:

$$\boldsymbol{Z}(f) = \boldsymbol{\Phi}^{-T}\begin{pmatrix} \ddots & & \\ & z_r & \\ & & \ddots \end{pmatrix}\boldsymbol{\Phi}^{-1} \tag{10}$$

where $z_r = k_r - f^2m_r + jfc_r$, jf is frequency at j-column.

The matrix of frequency response $\boldsymbol{H}(\omega)$ can be expressed as:

$$\boldsymbol{H}(f) = \boldsymbol{Z}(f)^{-1} \tag{11}$$

$$\boldsymbol{H}_{ij}(f) = \sum_{r=1}^{N} \frac{\phi_{ri}\phi_{rj}}{m_r(f_r^2 - f^2 + j2\varphi_r f_r f)} \tag{12}$$

$$f^2 = \frac{k_r}{m_r} \tag{13}$$

$$\varphi_r = \frac{c_r}{2m_r f_r} \tag{14}$$

where φ_r, f_r and ϕ_r are vibration mode at r-order mode, damping ratio and frequency, respectively; and m_r, c_r and k_r are mass, damping and stiffness at r-order, respectively.

$\boldsymbol{H}(f)$ is actually linear superposition of frequency response from the vibration pickup sensors. The frequency values of the first five orders were calculated by the measured data through the theories above. The corresponding frequencies are shown in Table 2.

Table 2. The frequency values of first five vibration modes.

Vibration Mode	1	2	3	4	5
f (Hz)	5.942	18.981	25.130	37.935	50.034

3. Finite Element Analysis

In this section, a finite element model of the concrete-encased frame-reinforced concrete core tube building is constructed based on fiber column element and layered shell element in OpenSees. OpenSees has the advantages of excellent nonlinear computation capacities and accurate simulation for elastic-plastic behavior of structures [33,34]. Reasonable constitutive relations and element types are respectively adopted and described as follows. The concrete and steel mechanical properties are related to the measured data.

3.1. Material Modeling

The "Concrete02" material as uniaxial concrete material object with tensile strength and linear tension softening is described by the curve as shown in Figure 7. The modified Kent–Park uniaxial concrete model is adopted for the material properties. Both unconfined and confined concrete fibers in this constitutive model consider tensile strength with linear degeneration. The strain–stress constitutive relationship can be expressed in Equations (15)–(18) [35].

$$\sigma = \begin{cases} f_c\left[\frac{2\varepsilon}{0.002} - \left(\frac{\varepsilon}{0.002}\right)^2\right] & \varepsilon \le 0.002 \\ f_c[1 - Z(\varepsilon - 0.002)] & 0.002 \le \varepsilon \le \varepsilon_{20} \\ 0.2f_c & \varepsilon \ge \varepsilon_{20} \end{cases} \tag{15}$$

$$Z = \frac{0.5}{\varepsilon_{50u} + \varepsilon_{50h} - 0.002} \tag{16}$$

$$\varepsilon_{50u} = \frac{3 + 0.002f_c}{0.002f_c - 1000} \tag{17}$$

$$\varepsilon_{50h} = \frac{3}{4}\rho_s\sqrt{\frac{B}{s_h}} \tag{18}$$

where σ is stress; ε is strain; f_c is compressive strength; ρ_s is stirrup ratio; B is width of core concrete; and s_h is stirrup spacing.

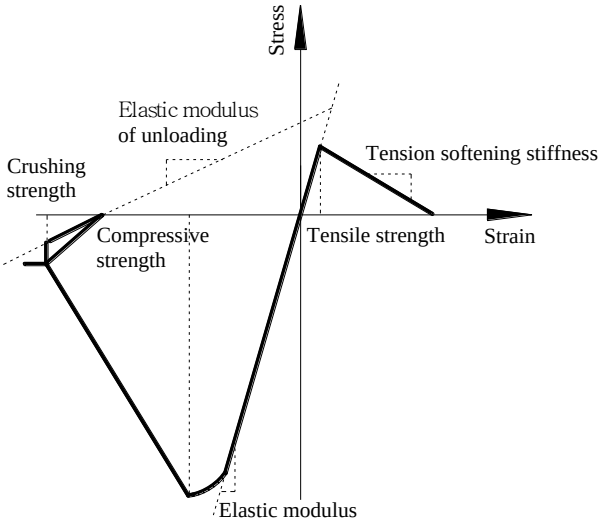

Figure 7. Stress–strain curve of concrete.

The "Steel02" material is in OpenSees, as uniaxial Giuffre–Menegotto–Pinto steel material objects with isotropic strain hardening are allocated to columns and beams. The von Mises yield criterion is used for steel. The stress–strain curve exhibits two stages, including elastic and hardening stages, as shown in Figure 8. The reinforcement element is embedded in concrete so that the strain of the reinforcement is compatible with that of concrete element [36]. E_s is elastic modulus of steel; f_y is yield strength; and E_p is the strain-hardening ratio and takes the value of 0.001 [37]. The "Steel02" material and "Concrete02" material take the properties which are with nonlinear stress–strain constitutive relations.

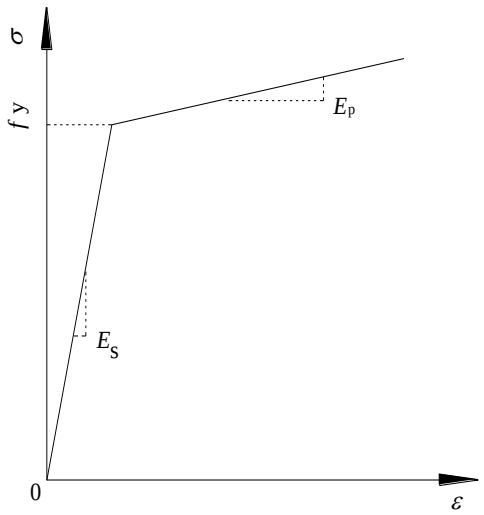

Figure 8. Stress–strain curve of steel, f_y: yield strength; E_p: strain-hardening ratio; E_s: elastic modulus of steel.

3.2. Elements of Component

The nonlinear beam–column element is adopted, which considers the effects of P-Δ and large deformations, which P and Δ are static load and displacement, respectively [38]. The extra inner forces will be transmitted to the surrounding elements of beam and column through the inner force redistribution. Therefore, reasonable material and element forms need to be selected. Columns and beams are simulated by "dispBeamColumn" element, which is a fiber element based on stiffness

method. Each element is divided into four integration points; the Gauss–Lobotto quadrature rule is adopted to integrate iteration as shown in Figure 9. Each point has corresponding weight function ω and distribution of integral point ξ. The beam section is assembled by material stiffness and stress by fibers at local coordinate system as illustrated in Figure 10 [39]; each fiber exhibits different constitutive material models.

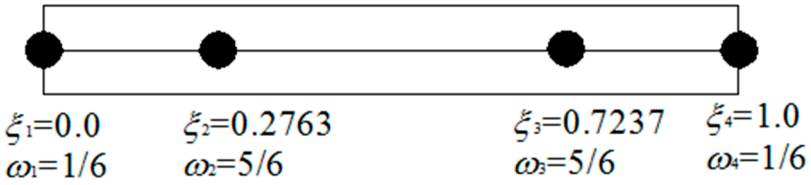

Figure 9. Distribution of integral points and weighting function.

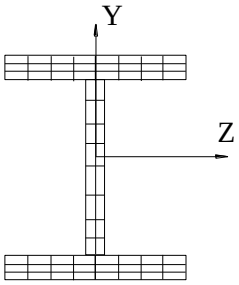

Figure 10. Fiber distributions in section of steel beam.

The shear wall is simulated by the "ShellMITC4" element. The "ShellMITC4" is a type of shell element in program, which is a bilinear isoparametric formulation to improve the thin-plate bending performance. It can account for the development of nonlinear membrane forces. The "LayeredShell" is adopted for the shear wall fiber section, which is based on the mechanics of composite materials. It considers the geometric nonlinearity of large deformations. A shell element is divided into several layers along the thickness direction and each layer is endowed appropriate material property to consider the coupling effect of bending and shear. The double-layer mesh reinforcement of core tube is treated as the equivalent steel layer. In the computational process the strain and curvature of the core layer are obtained, afterwards other layers are calculated according to the plane section assumption. The stress at each layer is solved by the respective constitutive equation of material. Finally, the inner force of shell element is educed by numerical integration. The longitudinal and transverse reinforcement is dispersed into the orthotropic reinforcement layer distributing uniformly in physical location, as illustrated in Figure 11 [40,41]. Table 3 shows the Component of model.

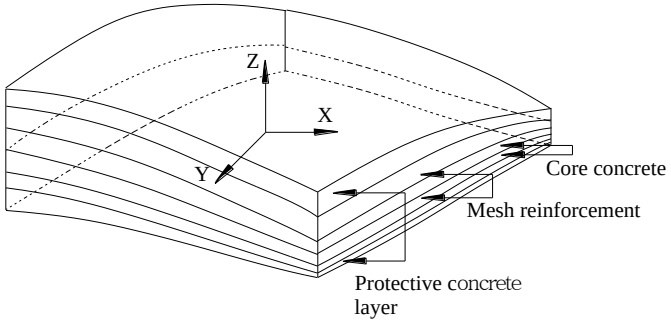

Figure 11. Schematic diagram of "LayeredShell".

Table 3. Component of model.

Item	Quantity
Node	340
"dispBeamColumn" element	420
"ShellMITC4" element	220

3.3. Comparison between Experimental Investigations and FEA

Finite element modal analysis is conducted on the experimental specimen. The sections and material properties are same as the test specimen. The damping percentage is 0.05 according to Code for Seismic Design of Buildings (GB50011-2001) of China. The first five order frequencies are calculated, which agree well with experimental results as shown in Table 4. Comparison between finite element result and test result indicates the accuracy of the finite element modal analysis.

Table 4. Comparison of frequencies, FEA: finite element modal analysis.

Order	Frequencies of Specimen (Hz)	Frequencies of FEA (Hz)	Absolute Error (%)
1	5.942	5.864	1.312
2	18.981	18.126	4.504
3	25.130	23.974	4.601
4	37.935	36.469	3.865
5	50.034	48.433	3.199

4. Seismic Damage Evaluation

4.1. Structural Damage Analysis under Earthquake Action

The El-Centro wave is selected as a representative ground motion input to investigate the damage process. Acceleration–time history and elastic response spectrum of El-Centro wave are shown in Figure 12. The analysis time increment is 0.02 s to ensure the accuracy and convergence. Fundamental period T_0 of specimen measured in the above experiment is 0.169 s, the corresponding acceleration in response spectrum is S_a = 0.67g, where g is acceleration of gravity. This intensity of earthquake is appropriate to reflect dynamic characteristics of hybrid structure [42,43]. Specimen experiences different degree of stiffness degradation, which eventually leads to the increase of period. Period-time history curves for the first seven vibration modes are shown in Figure 13.

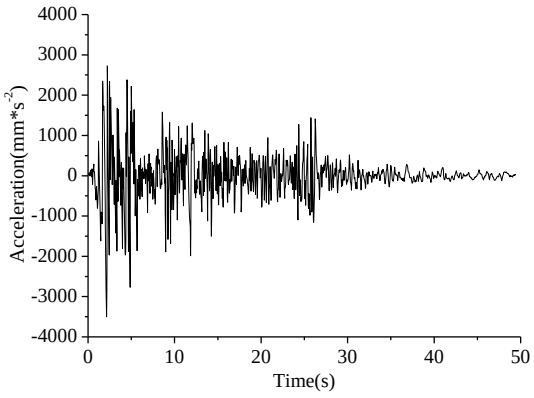

(**a**)

Figure 12. *Cont.*

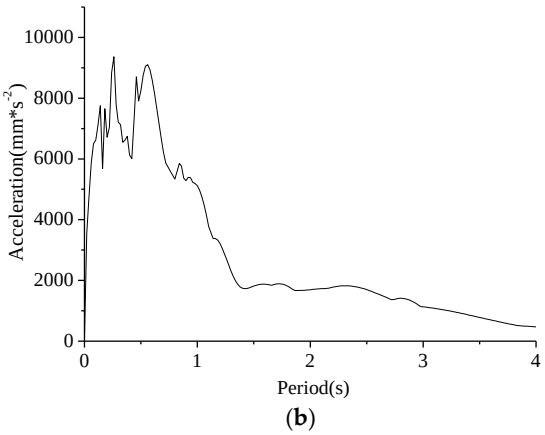

Figure 12. (**a**) Time history curve of acceleration of El-Centro wave; (**b**) response spectrum.

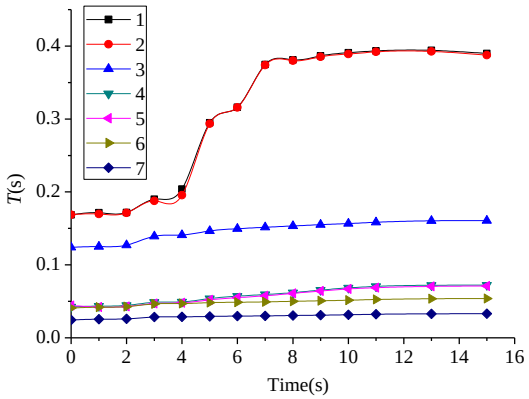

Figure 13. Time history curve of period for the first seven vibration modes.

Displacement-time history curves and acceleration-time history curves of the top node are shown in Figures 14 and 15. Furthermore, the total shear resisted by the columns and the core wall at the bottom are shown in Figure 16. At the initial stage when t = 1.2 s, periods of all vibration modes remain constant, no stiffness degradation occurs, and the core wall bears 53.37% of total shear. When t = 3.2 s, periods increase in varying degrees. Concrete-encased steel frame slightly damages and shear is redistributed to core wall. Lateral displacement of specimen increases gradually and reaches maximum. Subsequently when t = 4.8 s, periods increase rapidly especially in the first and the second vibration modes. Core wall resists 77.36% of the total shear.

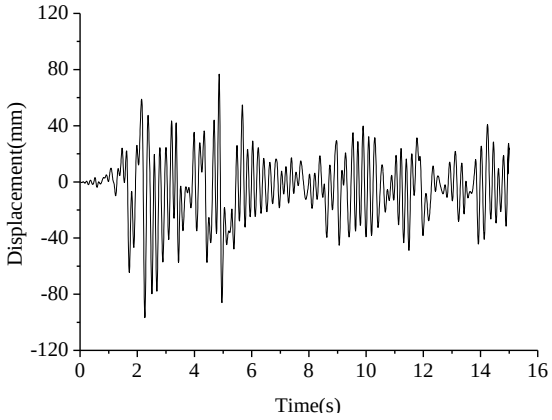

Figure 14. Displacement–time history curves.

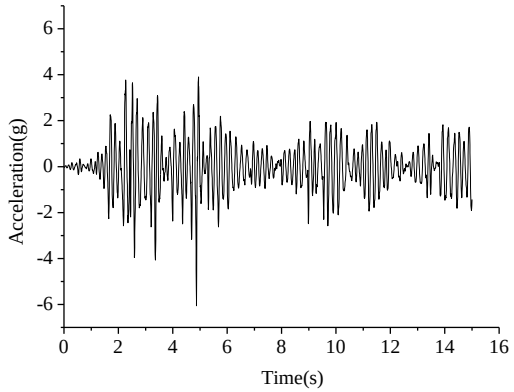

Figure 15. Acceleration–time history curves.

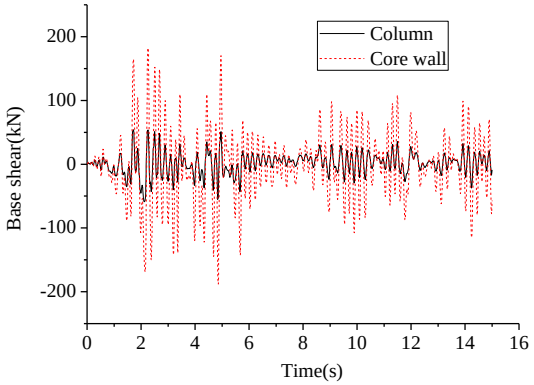

Figure 16. Shear distribution of columns and core wall at the bottom.

4.2. Criterion of Seismic Damage Assessment

According to Standard for Seismic Appraisel of Building (GB50023-2009) of China, structural damage is classified into five levels, as shown in Table 5 and Figure 17. D is the index for assessing damage of structure.

Table 5. Damage index (D) related to damage level.

Intact State	Minor Damage	Medium Damage	Serious Damage	Collapse
$D \leq 0.08$	$0.08 < D \leq 0.16$	$0.16 < D \leq 0.60$	$0.60 < D \leq 1.0$	$D > 1$

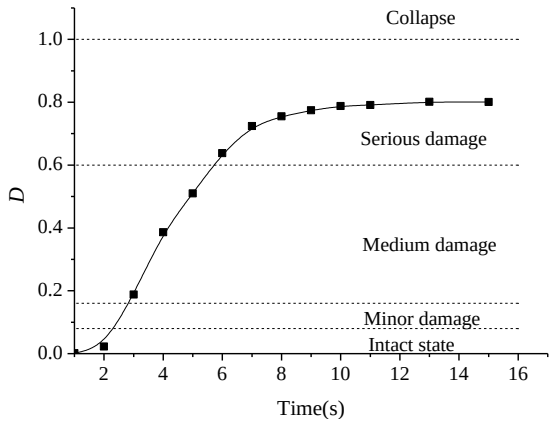

Figure 17. Seismic damage with the consideration of max story drift angle (θ_{max}).

The dynamic characteristics at each loading time including higher-order vibration modes are obtained by finite element modal analysis. Furthermore, the max story drift angle $\theta_{\max}$ was chosen to reflect the damage state and to quantify the damage degree. Seismic damage index at the end of each loading point is expressed as $D_\theta = 1 - \theta_{\max,0}/\theta_{\max,D}$, where D_θ is the damage index which considers max story drift angle $\theta_{\max}$. $\theta_{\max,0}$ and $\theta_{\max,D}$ are the max story drift angles at initial and damage stage, respectively.

The frequencies of the first seven vibration modes and D_θ at each loading stage are shown in Table 6. The results show the degradation of frequencies relating to loading history, which means different degrees of damage.

Table 6. Degradation of frequencies related to time history.

Time	Frequencies of Vibration Modes (Hz)							D_θ
	1	2	3	4	5	6	7	
1 s	5.833	5.888	7.999	22.957	23.691	23.895	39.124	0.00145
2 s	5.819	5.834	7.865	22.553	23.326	23.425	38.402	0.0227
3 s	5.266	5.328	7.184	20.534	21.277	21.459	35.088	0.18822
4 s	4.902	5.112	7.097	20.284	20.877	21.231	34.843	0.38641
5 s	3.392	3.407	6.826	18.622	19.231	20.704	34.130	0.50969
6 s	3.164	3.167	6.680	17.513	18.149	20.492	33.670	0.63802
7 s	2.670	2.675	6.592	16.835	17.361	20.284	33.223	0.72402
8 s	2.624	2.632	6.519	16.129	16.393	20.000	32.680	0.75483
9 s	2.587	2.595	6.447	15.267	15.576	19.724	32.154	0.77435
10 s	2.558	2.569	6.382	14.620	14.925	19.380	31.646	0.78807
11 s	2.542	2.550	6.310	14.162	14.548	19.048	31.027	0.79134
13 s	2.538	2.546	6.229	13.866	14.162	18.671	30.358	0.80114
15 s	2.565	2.580	6.221	13.856	14.077	18.574	30.184	0.80065

When specimen is subjected to the seismic load, severe damage occurs in frame and core tube. The degeneration of fundamental frequency is an important parameter to reflect structural damage. The common damage assessment based on natural frequency is expressed as Equation (19) [44].

$$D = 1 - \frac{f_i^2}{f_0^2} \tag{19}$$

where f_i and f_0 are the frequencies at damage and initial stage, respectively.

However, with the increase of structure height and the increase of irregularity, the influence of higher-order mode shapes cannot be neglected. In this paper, damage index D with the consideration of higher-order vibration modes is proposed as Equations (20)–(22), which considers structural form and frequency detection method [45].

$$D = 1 - \left(\sum_{i=1}^{m} \alpha_i \frac{f_i^2}{f_0^2} \right)^{\alpha\beta} \tag{20}$$

where α_i is weighted coefficient. It can be expressed as:

$$\alpha_i = (m + 1 - i) / \sum_{i=1}^{m} (m + 1 - i) \tag{21}$$

$$D = 1 - \left(\frac{2}{m+1} \sum_{i=1}^{m} \gamma_i \frac{f_i^2}{f_0^2} \right)^{\alpha\beta} \tag{22}$$

where m is the quantity of higher-order vibration modes; f_i is frequency at the loading time of i-th order vibration mode; γ_i is participation factor of the i-th vibration mode and can be calculated as $\gamma_i = (m + 1 - i)/m$; and α and β are influence coefficients associated with the structural form and frequency detection method, which take values of 1.0 and 1.2, respectively.

5. Seismic Damage Analysis

5.1. Influence of Earthquake Intensity

In order to adequately study the influence of ground motion parameters on the dynamic response of structure, the El-Centro wave was selected and eight suitable intensities were selected in the time history analysis. The main index δ = PGV/PGA was adopted to evaluate the seismic intensity, where PGV (Peak Ground-motion Velocity) and PGA (Peak Ground-motion Acceleration) are peak ground velocity and acceleration, respectively. Enough vibration modes m are taken into consideration and in this paper m = 10. Seismic damages of a concrete-encased steel frame-reinforced concrete core tube building under different intensity are evaluated, and the relationship of δ-D is shown in Figure 18.

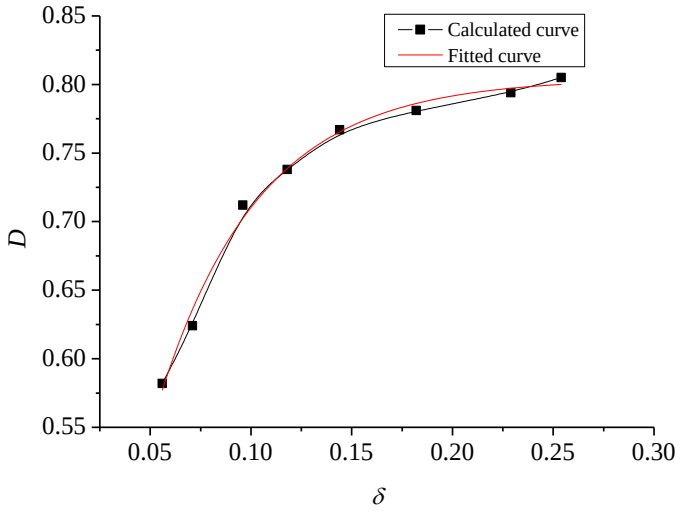

Figure 18. δ-D curve.

Fitting the curve above and equation can be expressed as Equation (23), where the determination coefficient ${R_1}^2$ is 0.990.

$$D = 0.804 - 0.697\mathrm{e}^{-\delta/0.049} \tag{23}$$

In general, D continuously increases with increase of δ. Structure rapidly damages when $\delta < 0.118$ and then experiences serious damage. Damage of the concrete-encased steel frame-reinforced concrete core tube building is sensitive to minor seismic intensity.

5.2. Structural Stiffness Ratio

The concrete encased steel frame and the reinforced concrete core tube are major components which bear the lateral force. Different structural stiffness leads to unequal distribution of the total lateral force. Structural stiffness ratio λ can be expressed as:

$$\lambda = H\sqrt{\frac{C_\mathrm{F}}{E_\mathrm{w} I_\mathrm{w}}} \tag{24}$$

$$C_\mathrm{F} = \eta\frac{12i}{H^2} \tag{25}$$

$$E_{\mathrm{w}} I_{\mathrm{w}} = \frac{E I_q}{1 + \frac{9\mu I}{H^2 A_{\mathrm{q}}}} \tag{26}$$

where H is height; C_{F} is the shear stiffness of column; η is the stiffness modified coefficient; i is the linear stiffness; $E_{\mathrm{w}} I_{\mathrm{w}}$ is the bending stiffness of shear wall; EI is the total stiffness; i is linear rigidity; and I is moment of inertia. In the analysis of the internal force and displacement of structures, the influence of shear deformation should be considered. The most effective and simple method is to multiply the bending stiffness $E_{\mathrm{w}} I_{\mathrm{w}}$ by a coefficient μ. μ is the shear-forced coefficient which takes value of 1.2 in rectangular cross section [46]; and A_{q} is the equivalent cross-sectional area.

The characteristics of lateral displacement curves are relatively different, as shown in Figure 19, which SRC frame and RC core tube are steel reinforced concrete frame and reinforced concrete core tube, respectively. Lateral deformation of hybrid structure μ is mainly influenced by structural stiffness ratio, as shown in Figure 20. The structure mainly performs property of bending as $\lambda \leq 1$ but property of shear as $\lambda \geq 6$.

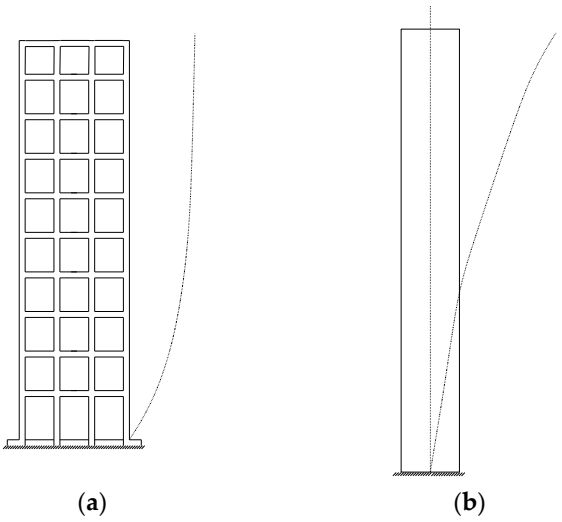

Figure 19. Lateral displacement curves: (**a**) SRC frame; (**b**) RC core tube.

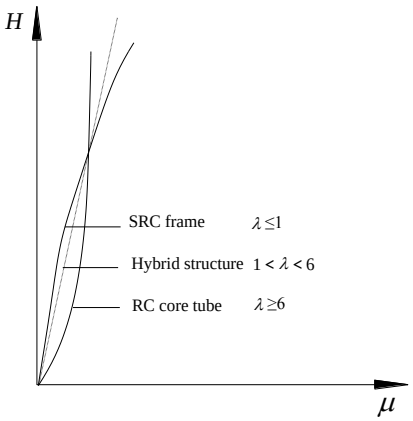

Figure 20. Comparison of lateral displacement curve, λ: structural stiffness ratio.

Fitting the curve in Figure 21 and the equation can be expressed as Equation (27), where the determination coefficient ${R_2}^2$ is 0.971.

$$D = \mathrm{e}^{-1.154 + 0.183\lambda - 0.007\lambda^2} \tag{27}$$

In contrast to the influence of δ, the hybrid structure had slight damage and experienced medium damage at $\lambda < 3.118$. However, the ultimate damage degree was slight less than that of δ.

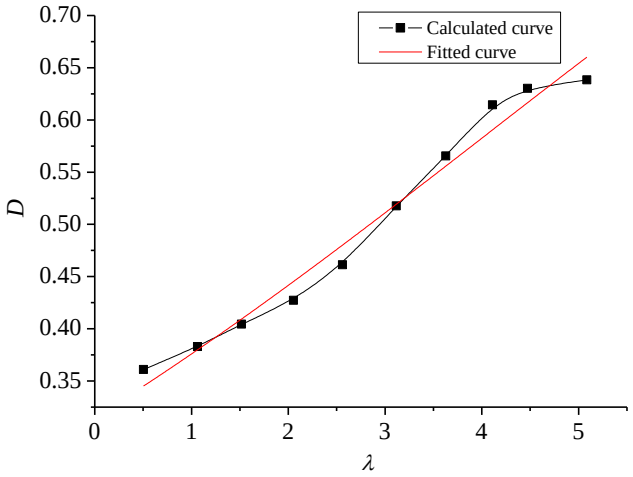

Figure 21. λ-D curve.

6. Conclusions

(1) A dynamic characteristics test was conducted on a 1/5 scale and 10-storey concrete-encased steel frame-reinforced concrete core tube building model. The natural frequency was measured by the high precision USB (Universal Serial Bus) acquisition instrument, and higher order frequencies through modal analysis were obtained. As a result, first five order frequencies were obtained according to experimental data.

(2) Modal analysis was carried out using a nonlinear finite element program based on the fiber model. The simulation results agreed well with those of experiments. The damage process under El-Centro wave was analyzed. Compared with the intact state, the first two frequencies of the ultimate state had an obvious degradation of about 56.16%, and the higher frequencies had an obvious degradation of about 21.87%. The max story drift angle increased from 0.819% to 4.062%, and the proportion of the total shear in the core tube increased from 53.37% to 77.36%.

(3) The max story drift angle was chosen to reflect the damage state and to quantify the damage degree on five levels. A criterion of seismic damage assessment was proposed with the consideration of higher-order vibration modes and its validity was confirmed by finite element analysis. The influence of earthquake intensity and structural stiffness ratio on dynamic characteristics were discussed. This work is hoped to provide references for structural health monitoring and quantifying the degree of post-earthquake restoration.

Acknowledgments: This research was funded by Natural Science Foundation of Hubei Province of China (Grant No. 2016CFB604), Natural Science Foundation of China (Grant Nos. 51108041, 51378077), Science Foundation of the Education Department of Hubei Province of China (Grant No. D20161305) and their support is gratefully acknowledged.

Author Contributions: Lei Zeng conceived and designed the experiments; Yunfeng Xiao and Siqian Jin performed the experiments; Yiguang Chen, Xianjie Li and Wei Xie analyzed the data; Yunfeng Xiao and Lei Zeng wrote the paper.

Conflicts of Interest: The authors declare no conflict of interest.

References

1. Shanmugam, N.E.; Lakshmi, B. State of the art report on steel-concrete composite columns. *J. Constr. Steel Res.* **2001**, *57*, 1041–1080. [CrossRef]

2. Nie, J.; Tao, M.; Huang, Y.; Tian, S.; Chen, G. Research advances of steel-concrete composite structural systems. *J. Build. Struct.* **2010**, *31*, 71–80.
3. Deierlein, G.G.; Noguchi, H. Overview of US-Japan research on the seismic design of composite reinforced concrete and steel moment frame structures. *J. Struct. Eng.* **2004**, *130*, 361–367. [CrossRef]
4. Goel, S.C. United States-Japan cooperative earthquake engineering research program on composite and hybrid structures. *J. Struct. Eng.* **2004**, *130*, 157–158. [CrossRef]
5. Zeng, L.; Cui, Z.K.; Xiao, Y.F.; Jin, S.Q.; Wu, Y.Y. Cyclical Behavior of Concrete-Encased Composite Frame Joints with High Strength Concrete. *Adv. Mater. Sci. Eng.* **2015**, *2015*, 873162.
6. Zheng, S.S.; Zeng, L. Experimental research on seismic behavior of steel reinforced high strength and high performance concrete frame joints. *J. Build. Struct.* **2008**, *29*, 74–81.
7. Zhou, X.; Li, G. Shaking table model test of a steel-concrete composite high-rise building. *J. Earthq. Eng.* **2010**, *14*, 601–625. [CrossRef]
8. Yang, Y.; Wang, P.; Wang, J.; Jin, X. Seismic analysis of the hung curtain wall structure in Shanghai Center Tower. *Struct. Des. Tall Spec. Build.* **2013**, *22*, 847–861. [CrossRef]
9. Lu, X.L.; Yin, X.W.; Jiang, H.J. Shaking table scaled model test on a high-rise building with CFT frame and composite core wall. *Eur. J. Environ. Civ. Eng.* **2013**, *17*, 616–634. [CrossRef]
10. Gong, Z.G.; Li, X.L.; Lu, W.S.; Li, P.Z.; Yang, S.; Zhao, B. Shaking table model test of a hybrid high-rise building structure. *Earthq. Eng. Eng. Vib.* **2004**, *24*, 99–105.
11. Zhou, F.; Mosalam, K.M.; Nakashima, M. Finite-element analysis of a composite frame under large lateral cyclic loading. *J. Struct. Eng.* **2007**, *133*, 1018–1026. [CrossRef]
12. Zona, A.; Ranzi, G. Finite element models for nonlinear analysis of steel–concrete composite beams with partial interaction in combined bending and shear. *Finite Elem. Anal. Des.* **2011**, *47*, 98–118. [CrossRef]
13. Sebastian, W.M.; McConnel, R.E. Nonlinear FE analysis of steel-concrete composite structures. *J. Struct. Eng.* **2000**, *126*, 662–674. [CrossRef]
14. Miao, Z.; Ye, L.; Guan, H.; Lu, X. Evaluation of modal and traditional pushover analyses in frame-shear-wall structures. *Adv. Struct. Eng.* **2011**, *14*, 815–836. [CrossRef]
15. Lu, X.; Lu, X.; Guan, H.; Ye, L. Collapse simulation of reinforced concrete high-rise building induced by extreme earthquakes. *Earthq. Eng. Struct. Dyn.* **2013**, *42*, 705–723. [CrossRef]
16. Shahrooz, B.M.; Gong, B.; Tunc, G.; Deason, J.T. An overview of reinforced concrete core wall–steel frame hybrid structures. *Prog. Struct. Eng. Mater.* **2001**, *3*, 149–158. [CrossRef]
17. Králik, J. Seismic analysis of reinforced concrete frame-wall systems considering ductility effects in accordance to Eurocode. *Eng. Struct.* **2010**, *31*, 2865–2872. [CrossRef]
18. Darwin, D.; Nmai, C.K. Energy dissipation in RC beams under cyclic load. *J. Struct. Eng.* **1986**, *112*, 1829–1846. [CrossRef]
19. Park, Y.J.; Ang, A.H.S.; Wen, Y.K. Seismic damage analysis of reinforced concrete buildings. *J. Struct. Eng.* **1985**, *111*, 740–757. [CrossRef]
20. Lu, X.; Lu, X.; Guan, H.; Ye, L. Earthquake-induced collapse simulation of a super-tall mega-braced frame-core tube building. *J. Constr. Steel Res.* **2013**, *82*, 59–71. [CrossRef]
21. Zeng, L.; Parvasi, S.M.; Kong, Q.; Huo, L.; Lim, I.; Li, M.; Song, G. Bond slip detection of concrete-encased composite structure using shear wave based active sensing approach. *Smart Mater. Struct.* **2015**, *24*, 125026. [CrossRef]
22. Xu, B.; Zhang, T.; Song, G.; Gu, H. Active interface debonding detection of a concrete-filled steel tube with piezoelectric technologies using wavelet packet analysis. *Mech. Syst. Signal Process.* **2013**, *36*, 7–17. [CrossRef]
23. Xu, B.; Li, B.; Song, G. Active Debonding Detection for Large Rectangular CFSTs Based on Wavelet Packet Energy Spectrum with Piezoceramics. *ASCE J. Struct. Eng.* **2013**, *139*, 1435–1443. [CrossRef]
24. Huang, Q.; Xu, B.; Li, B.; Song, G.; Teng, J. Monitoring for large cross-section CFSTs of a super high-rise building with piezoceramic actuators and sensors. *Adv. Mater. Res.* **2011**, *163–167*, 2553–2559. [CrossRef]
25. Gu, H.; Moslehy, Y.; Sanders, D.; Song, G.; Mo, Y.L. Multi-functional smart aggregate-based structural health monitoring of circular reinforced concrete columns subjected to seismic excitations. *Smart Mater. Struct.* **2010**, *19*, 322–328. [CrossRef]
26. Qin, F.; Kong, Q.; Li, M.; Mo, Y.; Song, G.; Fan, F. Bond slip detection of steel plate and concrete beams using smart aggregates. *Smart Mater. Struct.* **2015**, *24*, 115039. [CrossRef]

27. Laskar, A.; Gu, H.; Mo, Y.L.; Song, G. Progressive collapse of a two-story reinforced concrete frame with embedded smart aggregates. *Smart Mater. Struct.* **2009**, *18*, 5844–5877. [CrossRef]
28. Kong, Q.; Robert, R.H.; Silva, P.; Mo, Y.L. Cyclic crack monitoring of a reinforced concrete column under simulated pseudo-dynamic loading using piezoceramic-based smart aggregates. *Appl. Sci.* **2016**, *6*, 341. [CrossRef]
29. Yin, H.; Wang, T.; Yang, D.; Liu, S.; Shao, J.; Li, Y. A smart washer for bolt looseness monitoring based on piezoelectric active sensing method. *Appl. Sci.* **2016**, *6*, 320. [CrossRef]
30. Shao, J.; Wang, T.; Yin, H.; Yang, D.; Li, Y. Bolt looseness detection based on piezoelectric impedance frequency shift. *Appl. Sci.* **2016**, *6*, 298. [CrossRef]
31. Zhu, W.D.; Liu, J.M.; Xu, Y.F.; Yin, H.Q. A modal test method using sound pressure transducers based on vibro-acoustic reciprocity. *J. Sound Vib.* **2014**, *333*, 2728–2742. [CrossRef]
32. Kang, H.J.; Zhao, Y.Y.; Zhu, H.P. Analytical and experimental dynamic behavior of a new type of cable-arch bridge. *J. Constr. Steel Res.* **2014**, *101*, 385–394. [CrossRef]
33. Jiang, B.C.; He, Z.; Zhu, S. OpenSees-based master-slave modeling technique in progressive collapse analysis of concrete structures. *J. Disaster Prev. Mitig. Eng.* **2014**, *34*, 632–636.
34. Fanaie, N.; Ezzatshoar, S. Studying the seismic behavior of gate braced frames by incremental dynamic analysis (IDA). *J. Constr. Steel Res.* **2014**, *99*, 111–120. [CrossRef]
35. Kent, D.C.; Park, R. Flexural Members with Confined Concrete. *J. Struct. Div.* **1971**, *97*, 1969–1990.
36. Wu, Y.T.; Kang, D.Y.; Yang, Y.B. Seismic performance of steel and concrete composite shear walls with embedded steel truss for use in high-rise buildings. *Eng. Struct.* **2016**, *125*, 39–53. [CrossRef]
37. Chen, X.W.; Lin, Z. *Structural Nonlinear Analysis Program Opensees Theory and Tutorial*; China Architecture & Building Press: Beijing, China, 2014; pp. 87–89.
38. Kamaris, G.S.; Skalomenos, K.A.; Hatzigeorgiou, G.D.; Beskos, D.E. Seismic damage estimation of in-plane regular steel/concrete composite moment resisting frames. *Eng. Struct.* **2016**, *115*, 67–77. [CrossRef]
39. Spacone, E.; Eltawil, S. Nonlinear Analysis of Steel-Concrete Composite Structures: State of the Art. *J. Struct. Eng.* **2004**, *130*, 159–168. [CrossRef]
40. Arshian, A.H.; Morgenthal, G.; Narayanan, S. Influence of modelling strategies on uncertainty propagation in the alternate path mechanism of reinforced concrete framed structures. *Science* **2016**, *802*, 241–245. [CrossRef]
41. Vigh, L.G.; Deierlein, G.G.; Miranda, E.; Liel, A.B.; Tipping, S. Seismic performance assessment of steel corrugated shear wall system using non-linear analysis. *J. Constr. Steel Res.* **2013**, *85*, 48–59.
42. Tirca, L.; Chen, L.; Tremblay, R. Assessing collapse safety of CBF buildings subjected to crustal and subduction earthquakes. *J. Constr. Steel Res.* **2015**, *115*, 47–61. [CrossRef]
43. Pucinotti, R.; Bursi, O.S.; Demonceau, J.F. Post-earthquake fire and seismic performance of welded steel–concrete composite beam-to-column joints. *J. Constr. Steel Res.* **2011**, *67*, 1358–1375. [CrossRef]
44. Shen, W.H. Structural Damage Detection Based on Experimental Modal Analysis. Master's Thesis, Jinan University, Guangzhou, China, 2006.
45. Shi, W.X.; Wang, Y.; Liu, C.Q. Damage analysis of high-rise building under seismic load based on frequency measurement. *J. Southwest Jiaotong Univ.* **2007**, *42*, 389–394.
46. Tao, Q.L. Research on the Damage Model of SRC Frame-RC Core Wall Hybrid Structure under Seismic Excitation. Ph.D. Thesis, Xi'an University of Architecture and Technology, Xi'an, China, 2011.